CORROSION DEGRADATION STUDY OF SHELL AND TUBE HEAT EXCHANGERS IN PETROCHEMICAL PLANTS

STUDIUL DEGRADĂRII PRIN COROZIUNE A SCHIMBĂTORULUI DE CĂLDURĂ CU MANTA ȘI TUBURI DIN CADRUL INSTALAȚIILOR PETROCHIMICE

Mihai OPREA[1], Ion Nae[2], Gabriela Cristina IONESCU[3], Răzvan George RÎPEANU[4], Ibrahim Naim RAMADAN[5]

Abstract: *This paper presents the research results carried out to evaluate the degradation and lifespan of a heat exchanger used for heating salt water (containing hydrocarbon traces) within a petrochemical plant. Initial static tests, including corrosion tests, were performed, followed by an investigation into the most common failures and their mechanisms affecting the heat exchanger's shell and tubes. Corrosion testing indicated susceptibility to pitting corrosion, particularly at elevated temperatures. Finally, methods for monitoring heat exchanger performance were proposed.*

Keywords: shell and tube heat exchanger, corrosion testing, shell, tubes.

Rezumat: *Lucrarea prezentă rezultatele cercetărilor realizate în scopul evaluării degradării și duratei de viață a schimbătorului de căldură utilizat la încălzirea apei sărate (cu urme de hidrocarburi) din componența unei instalații petrochimice. Au fost efectuate teste statice inițiale care cuprind teste de coroziune și apoi s-au cercetat cele mai frecvente defecțiuni și mecanismele*

[1] PhD Student, Dept. of Mechanical Engineering, Petroleum - Gas University of Ploiesti, e-mail: oprea_mihai94@yahoo.
[2] Prof. habil. dr. eng., Dept. of Mechanical Engineering, Petroleum - Gas University of Ploiesti, e-mail: inae@upg-ploiești.ro
[3] Assoc. Prof. dr., eng., Dept. of Mechanical Engineering, Petroleum - Gas University of Ploiesti, e-mail: ionescug@upg-ploiești.ro
[4] Prof. habil. dr. eng., Dept. of Mechanical Engineering, Petroleum - Gas University of Ploiesti, e-mail: rrapeanu@upg-ploiesti.ro
[5] Assoc. Prof. dr., eng., Dept. of Mechanical Engineering, Petroleum - Gas University of Ploiesti, e-mail: ibra@upg-ploiesti.ro

acestora asupra mantalei și țevilor schimbătorului de căldură. Testele de coroziune a indicat susceptibilitatea la coroziune prin pitting mai ales la temperaturi ridicate. În final, au fost propuse metode de monitorizarea performanței schimbătorului de căldură.

Cuvinte cheie: schimbător de căldură cu manta și tuburi, teste de coroziune, manta, țevi.

1. Introduction

Shell-and-tube heat exchangers represent critical infrastructure components across major industrial sectors, including power generation, chemical processing, petrochemicals, and the pulp and paper industry. The primary function of such equipment is to ensure efficient thermal transfer between two distinct fluid media [1,2].

Although this equipment is widely utilized, its operational reliability remains constrained by degradation phenomena occurring during service. Manufacturers and operators frequently encounter in-service failures, primarily driven by temperature gradients, fouling phenomena, and corrosion processes.

Corrosion induces a progressive and continuous degradation of the metallic matrix and its associated alloys, resulting from chemical or electrochemical interactions with aggressive working environments. The manifestations of this process include pitting, macroscopic cracking, and other forms of localized deterioration. Furthermore, the synergy between the chemical attack of corrosive fluids and tensile mechanical stresses (both residual and operational) promotes stress corrosion cracking (SCC), thereby accelerating the structural collapse of the equipment

Carbon steel remains the most frequently utilized material in oil and petrochemical industry applications. Yong Hua et al. [3] investigated the susceptibility of carbon steel to various forms of corrosion. The studies reveal that the plurality of kinetic and structural mechanisms governing iron sulphide (FeS) formation represents a fundamental aspect that is still insufficiently elucidated in the literature, particularly regarding the dynamics of multiphase systems (H_2S/CO_2). The localized and/or pitting corrosion process of carbon steel constitutes a critical structural integrity issue. Linear polarization resistance (LPR) measurements combined with post-experimental surface analyses, such as XRD and SEM, are utilized to understand the nuances of both localized and general corrosion behavior.

Masayuki Sagara et al. [4] investigated corrosion-resistant alloys (CRAs), specifically austenitic materials (API 5CRA / ISO 13680), under exploration and production conditions characterized by high pressures and high temperatures (HPHT), where the processed media contain significant amounts of hydrogen sulphide, carbon dioxide, and chloride ions. Surface films on conventional UNS N08535 CRAs were analysed. The film formed after long-term exposure inside an actual operating well was compared with that formed during laboratory corrosion tests.

Corrosion under insulation (CUI) represents a critical structural integrity issue for industrial equipment. Kentaro Mizushima et al. [5] conducted a comparative study on the effectiveness of various hybrid configurations (combinations of protective coatings and thermal insulation types) in preventing and controlling corrosion under insulation.

Document [6] provides a comparative evaluation of the requirements in international codes and standards regarding the mandate of post-forming heat treatments (such as stress relieving or annealing) applied to shell-and-tube heat exchanger components, with a particular focus on the critical region of U-bent tubes.

Study [7] analyzes how computational fluid dynamics (CFD) simulation serves as a critical and highly efficient tool for identifying the root causes of tube bundle failures in heat exchangers. The discussed case studies demonstrate that poor flow distribution generates recirculation zones and reduced fluid velocities, which correlate directly with localized increases in wall temperature and accelerated corrosion (wall thinning).

Jeffrey Xie et al. [8] investigated the severe degradation via pitting corrosion of carbon steel heat exchanger tubes caused by distinct corrosive mechanisms. To eliminate the risk of failure, they recommend optimizing cooling water hydrodynamics, controlling thermal agent quality, increasing the tube pitch, or upgrading the material to duplex stainless steel.

Zeynab Mahidashti et al. [9] analyzed the corrosion failure of heat exchanger tubes in petrochemical refineries, identifying carbon dioxide dissolved in crude methanol as the primary agent of electrochemical corrosion.

Work [10] investigates the applicability limits of the UNS N08904 alloy in chloride environments - restricted by ISO 15156-3 to H_2S partial pressures up to 0.1 MPa - through long-term (720 h) experimental testing in highly acidic brines. Specimen exposure at 90% of the yield strength demonstrated remarkable resistance: no cracking occurred, and the corrosion rate remained negligible (1…7 μm/year), even under galvanic influence.

Gerit Siegmund et al. [11] investigated the stress corrosion cracking resistance of UNS S31635 (AISI 316Ti) stainless steel. Specimens with a hardness of 23 HRC were tested at room temperature for 720 hours under tensile loads of 70% and 90% of the actual yield strength (AYS) and immersed in brine containing 1 g/l and 30 g/l of chlorides, respectively. No specimen exhibited cracking or localized degradation, and the overall corrosion rates remained extremely low (0.4...4 μm/year). The results demonstrate that this material can be safely utilized at room temperature in sour environments with up to 16 bar H_2S and chloride concentrations up to 30 g/l.

Cathodic protection represents one of the most effective methods for preventing corrosion in both aboveground and underground metallic structures [12]. This technology is widely utilized to protect critical assets such as pipelines, offshore platforms, vessels, subsea equipment, and various storage tanks intended for crude oil, petroleum products, or other liquids.

Paper [13] analyses a case of failure via stress corrosion cracking (SCC) of an austenitic stainless steel, discussing the implications of this event on current ISO regulations and recently proposed modifications.

In contrast to the approaches mentioned in the literature, the present work focuses on analysing the behavior of steels exposed to the action of wash water with hydrocarbon traces. Thus, it supplements existing data regarding the determination of the corrosion rate of reference materials (P265GH and X2CrNiMo17-12-2) utilized in the fabrication of the heat exchanger shell and subjected to the influence of specific working fluids. Furthermore, experimental research dedicated to evaluating the corrosion process is presented, conducted on specimens sampled during repair work performed on the shell of the studied equipment.

2. Technical Characteristics of the Shell-and-Tube Heat Exchanger

The structural integrity and lifetime evaluation of the studied heat exchanger are directly influenced by the compatibility between the chosen design solution and the chemical characteristics of the processed fluids. The equipment under investigation is a shell-and-tube heat exchanger (standardized according to TEMA standards – Figure 1), designed to operate under severe temperature and pressure conditions. To establish the dynamics of localized degradation processes, it is necessary to correlate the geometric parameters of the equipment with the hydrodynamic regime of the processed fluids.

Exchanger under maintenance / repair

Heat exchanger after repair / maintenance

Fig.1. Shell-and-tube heat exchanger.

Table 1 summarizes the technical characteristics of the studied heat exchanger.

Table 1. **Technical specifications of the heat exchanger**

Technical specifications	Shell	Tubes
Maximum Allowable Working Pressure	2.4 MPa (24 bar)	1.6 MPa (16 bar)
Maximum Allowable Temperature	145 ^{0}C	180 ^{0}C
Minimum Allowable Temperature	15 ^{0}C	15^{0}C
Test pressure	3.45 MPa (34.5 bar)	2.45 MPa (24.5 bar)
Process fluid	Wash water	Produced water (with hydrocarbon traces)
Volume	1.1 m^3	0.5 m^3
Number of passes	1	4
Dimensions (outer diameter/thickness)	508 mm/ 12 mm	-
Material specification (EN 10216-2/ ASME)	P265HG/ ASTM A106 Grade B	P265HG/ ASTM A106 Grade B
Thermal insulation	50 mm	-
TEMA type designation	AET	
TEMA class	R	

3. Experimental Testing Program

The experimental testing program addresses two primary objectives:

a) Determination of the corrosion rate through long-term laboratory testing. This stage aims to evaluate the behavior of two steel categories exposed

to the action of the working fluid (conventionally designated as F1). The P265GH material represents the carbon steel from which the current heat exchanger shell is fabricated, whereas the X2CrNiMo17-12-2 stainless steel is investigated as a technical replacement solution to optimize structural resistance.

b) Degradation assessment on actual industrial samples. Experimental research is presented on specimens sampled directly from the shell and tubes following the repair and maintenance work performed on the analyzed equipment.

Considering the mechanical design of the heat exchanger (comprising the shell and the tube bundle), the mechanical properties of the two steels (P265GH and X2CrNiMo17-12-2), and the chemical properties of the processed medium, the experimental program (Table 2) was configured to establish the corrosion rate of the reference materials in the presence of fluid F1 (Table 3).

Table 2. **Experimental corrosion research program**

Equipment	Component	Material	Working fluid	Number of specimens used	Coding
Heat exchanger	Shell, tubes	P265GH EN 10216-2:2024 (Symbol P)	F1	E1 E2	PE1F1 PE2F1
		X2CrNiMo17-12-2 EN 10216-5:2024 (Symbol X)	F1	E1 E2	XE1F1 XE2F1

Table 3. **Composition of the F1 working medium**

Ammonium	Fe	Na	Cr	Ni	Ca
25.20 [mg/l]	0.068 [mg/kg]	0.131 [mg/kg]	<0.04 [mg/kg]	<0.08 [mg/kg]	0.022 [mg/kg]

Ammonium	K	Mg	pH	S^{2-}	H_2S	C^-
25.20 [mg/l]	0.085 [mg/kg]	<0.01 [mg/kg]	9.37	4.81 [mg/l]	0.011 [mg/l]	34.08 [mg/l]

4. Methodology and technical conditions for conducting laboratory testing

The gravimetric method was utilized to evaluate the corrosion resistance.

4.1. Principle of the method

The quantitative determination of corrosion effects was carried out using gravimetric analysis, a method based on the mass changes of the specimens immersed in a specified medium. In evaluating the corrosion rate using the gravimetric method, the change in mass per unit area and unit time defines the gravimetric index, V_{Cg} (expressed in g/mm²·h). This index is determined using equation (1):

$$V_{Cg} = \pm \Delta m / (S \times t), \quad (1)$$

where: Δm represents the specimen mass change (g); S – the specimen surface area (mm²); t – the duration of the corrosion process (h).

The sign of the gravimetric index indicates the nature of the phenomenon: positive values (+) quantify the accumulation of corrosion products on the surface (mass gain), while negative values (-) reflect anodic dissolution or scale spallation (mass loss).

If the corrosion phenomenon manifests uniformly across the entire surface, the penetration index, I_p, can be calculated. This index expresses the average reduction in specimen thickness per unit time, is measured in mm/year, and is calculated using equation (2):

$$I_p = (V_{Cg} \times 24 \times 365) / \rho_m \text{ (mm/year)}, \quad (2)$$

where: V_{Cg} represents the gravimetric index (g/mm²·h); ρ_m – the density of the investigated material (g/mm³); 24 – the number of hours in a day; 365 – the number of days in a year.

Furthermore, to determine the corrosion rate (mm/year) in accordance with the ASTM G31-72 (2014) standard for laboratory immersion testing, equation (3) is applied:

$$V_C = K \times \Delta m / (S \times t \times \rho_m) \text{ (mm/year)}. \quad (3)$$

where: V_C represents the corrosion rate (mm/year); K – a conversion coefficient with a value of $8{,}76 \times 10^4$; Δm – the mass loss (g) which is determined as: $\Delta m = m_0$ (initial specimen mass) – m_i (final specimen mass); S – the specimen surface area (cm²); ρ_m – the material density (g/cm³); t – the immersion time (h).

4.2. Determination of the test specimen type

The test specimens are plate-type (Figure 2). Two categories of materials were used for the fabrication of the specimens: P265GH EN 10216-2:2024 and X2CrNiMo17-12-2 EN 10216-5:2024. A total of 4 specimens were machined and codified according to Table 2.

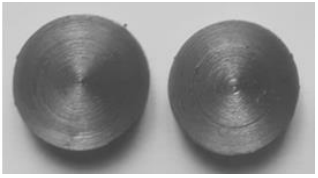

P265GH

X2CrNiMo17-12-2

Fig. 2. Test specimens used for the corrosion evaluation.

The sampling and mechanical machining operations of the specimens were carried out under optimized cutting regimes (reduced speed and feed rate), ensuring the preservation of the material's original microstructure and avoiding the induction of residual stresses.

4.3. Experimental determinations

The specimens were cleaned in an ethyl alcohol bath, degreased with distilled water, and weighed using a Mettler H35 analytical balance (Figure 3) with a precision of 0.0001 g.

The specimens are prepared for insertion into the test vessels (Figure 4). Subsequently, the specimens are immersed in the vessels containing the F1 working fluid (Figure 5).

Regarding the testing methodology, the procedure is as follows:

- the geometric dimensions of the test specimen are determined (d – diameter and h – thickness);
- the specimen surfaces are cleaned using methyl ethyl ketone (MEK);
- the specimen is weighed prior to testing to determine the initial mass, m_0;
- the specimen is prepared for testing and immersed in the vessel where the test solution has been poured;

- the total testing duration was t = 1632 h;
- following this period, the specimen is removed from the test vessel, cleaned, and weighed to determine the final mass, m_i;
- the gravimetric wear (mass loss) is determined using equation (4):

$$u_i = m_0 - m_i \tag{4}$$

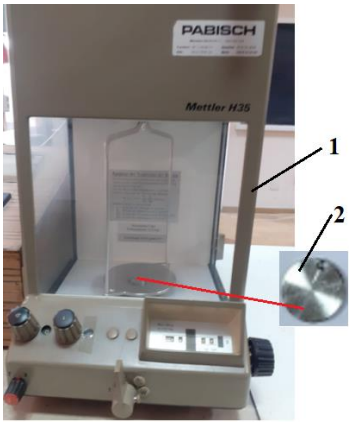

Fig. 3. Mettler H35 analytical balance:
1 – analytical balance;
2 – specimen.

P265GH X2CrNiMo17-12-2

Fig. 4. Corrosion specimens prepared for insertion into the working fluid.

Fig. 5. Immersion of specimens into the test vessels.

The tests were conducted at ambient temperature and a relative humidity of U = 40%.

4.4. Analysis and interpretation of results

The records obtained during the experiments consisted of determining the specimen masses (m_0 and m_i) and measuring their geometric dimensions (d – diameter and h – thickness). The achieved results are systematized in Table 4.

Considering the recorded experimental data, the gravimetric index V_{Cg} (equation 1), the penetration index Ip (equation 2), and the corrosion rate V_c (equation 3) were calculated. The obtained results are presented in Table 5.

Table 4. **Records of the results obtained from the corrosion resistance evaluation using the gravimetric method**

Specimen code	Material / Specimen	Fluid type	Specimen geometric dimensions		Specimen mass	
			Diameter, d	Thickness, h	Before m_0	After m_i
			[mm]	[mm]	[g]	[g]
PE1F1	P265GH 	F1	20.15	3.12	7.4264	7.3106
PE2F1	P265GH 	F1	19.97	3.24	7.3476	7.2426
XE1F1	X2CrNiMo17-12-2 	F1	19.97	2.96	6.8628	6.8018
XE2F1	X2CrNiMo17-12-2 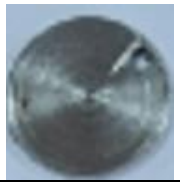	F1	20.24	3.11	7.1613	7.0734

Table 5. **Centralization of experimental data and corrosion rates for the analyzed specimens**

Specimen code	Material	Fluid type	Immersion time	Initial mass, m_0	Mass after immersion m_i	Mass change, Δm	Specimen geometric dimensions		Specimen surface area, S	Gravimetric index, V_{Cg}	Penetration index, Ip	Corrosion rate, Vc
							d	h				
			[h]	[g]	[g]	[g]	[mm]	[mm]	[mm^2]	[g/mm^2·h]	[mm/year]	[mm/year]
PE1F1	P265GH	F1	1632	7.4264	7.3106	0.1158	20.15	3.12	834.861	8.4991E-08	0.09484376	0.09484376*
PE2F1	P265GH	F1	1632	7.3476	7.2426	0.105	19.97	3.24	829.284	7.7583E-08	0.08657654	0.08657654*
XE1F1	X2CrNiMo17-12-2	F1	1632	6.8128	6.8018	0.011	19.97	2.96	811.727	8.3035E-09	0.0092661	0.0092661**
XE2F1	X2CrNiMo17-12-2	F1	1632	7.1108	7.1012	0.0096	20.24	3.11	840.814	6.996E-09	0.00780702	0.00780702**
	*) The average corrosion rate for the specimens fabricated from P265GH is $\underline{Vc,_P}$ = 0,09071015 [mm/year] **) The average corrosion rate for the specimens fabricated from X2CrNiMo17-12-2 is $\underline{Vc,_X}$ = 0,00853656 [mm/year]											

Subsequently, the graphical representations (Figure 6) are displayed, highlighting the variation of the corrosion rate as a function of the used material category (P265GH, X2CrNiMo17-12-2), the working fluid type (F1), and the specimen code (PE1F1, PE2F1, XE1F1, XE2F1).

Analyzing the centralized data in Table 4, Table 5, and Figure 6, it is found that the specimens fabricated from P265GH steel recorded the highest mass loss ($\Delta m,_P$ = 0.1158 g) and, implicitly, the highest corrosion rate ($V_{Cg,P}$ = 0.09071 mm/year) compared to the X2CrNiMo17-12-2 stainless steel, for which a mass loss ($\Delta m,_X$ = 0.0096 g) and a corrosion rate (V_{Cg} = 0.00853 mm/year) were determined for the immersion time of 1632 hours.

Analysis of the centralized data in Tables 4 and 5, as well as in Figure 6, indicates that the specimens fabricated from P265GH steel recorded the highest mass loss, $\Delta m,_P$ = 0.1158 g, and, implicitly, the highest corrosion rate ($V_{Cg,P}$ = 0.09071 mm/year).

By comparison, for the X2CrNiMo17-12-2 steel, after an immersion time of 1632 hours, a significantly lower mass loss ($\Delta m,_X$ = 0.0096 g) and a corrosion rate of (V_{Cg} = 0.00853 mm/year) were determined.

The comparative analysis of the specimens exposed for 1632 hours in the F1 medium (pH 9.37) reveals a corrosion rate that is 10.6 times higher for the P265GH carbon steel ($V_{Cg,P}$ = 0.09071 mm/year) compared to the X2CrNiMo17-12-2 stainless steel ($V_{Cg,X}$ = 0.00853 mm/year). The superior performance of the stainless steel is attributed to the passive chromium oxide (Cr_2O_3) layer and the presence of molybdenum, which neutralize the chloride and sulphide ions, whereas the carbon steel undergoes accelerated generalized degradation.

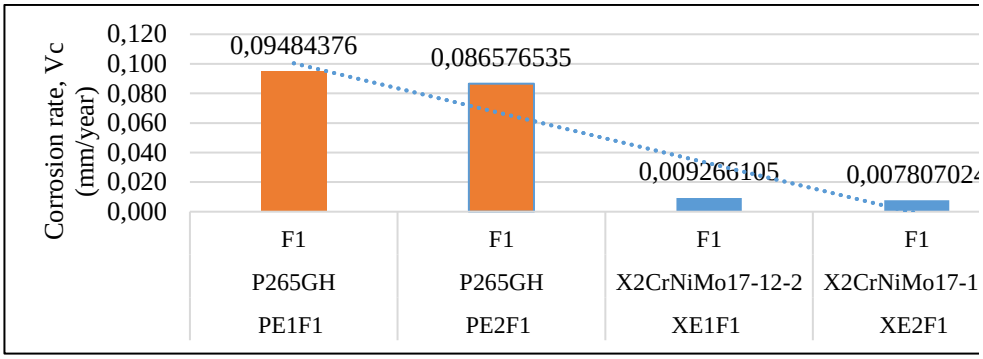

Fig. 6. Variation of the corrosion rate (*Vc*) as a function of material type, specimen code, and working fluid.

Table 6 synthesizes the obtained experimental data, highlighting the superiority of the X2CrNiMo17-12-2 material within the specified working medium.

Table 6. **Comparison between specimens (PE1F1, PE2F1) and (XE1F1, XE2F1)**

Technical characteristic	**P265GH**	**X2CrNiMo17-12-2**	**Impact on the test (1632 hours)**
Classification	Unalloyed carbon steel	High-alloy stainless steel	Radically changes the mode of reaction with the environment
Passivation layer	Absent (forms porous rust)	Present (Cr_2O_3), compact and protective)	Inhibits the corrosion kinetics of the symbol X specimens
Corrosion rate, V_{Cg}	0.09071 mm/year ((high)	0.00853 mm/year (negligible)	The symbol X specimen is ~10.6 times more resistant
Mass loss, Δm	0.1158 g	0.0096 g	The symbol P specimen lost ~12 times more mass

Regarding the X2CrNiMo17-12-2 steel, the obtained corrosion rate values confirm the trends identified in the literature for this type of material [10].

The analysis of the corrosion behavior and surface microstructure of the investigated specimens allows for the establishment of the following aspects.

Corrosion behavior of P265GH steel in fluid F1 (1632-hour test)

a. *Macroscopic analysis of the surfaces of the studied specimens***.** Examination of the surfaces of the P265GH steel specimens, conducted after the removal of the corrosion products, revealed the following:

- *Mode of corrosion manifestation***.** The surface does not exhibit uniform wear, but rather a pronounced alveolar attack (pitting) and under-deposit corrosion (Figure 7, specimen PE1F1).
- *Amplified cumulative effect of chlorides and sulphides***.** Chloride ions present in a high concentration (34.08 mg/l) locally penetrated the iron sulphide layer, initiating micro-pits. The 1632 h exposure duration favoured the propagation of these pits into the depth of the material.

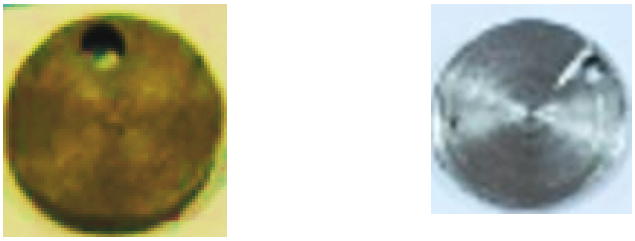

Specimen PE1F1 Specimen XE2F1

Fig. 7. Macroscopic analysis of the surfaces of the specimens immersed in fluid F1, immersion time t = 1632 h.

b. Extrapolation of laboratory results to real operating conditions – maximum allowable pressure of 2.4 MPa, maximum allowable temperature of 145 °C. Extrapolation of the corrosion rate based on the Arrhenius law [15–17] is based on the assumption that the corrosion process is controlled by a chemical or electrochemical reaction whose rate depends exponentially on temperature. The corrosion rate determined in the laboratory at ambient temperature ($T_1 \approx 20^0$C $\approx$ 293.15 K) is low ($V_{Cg,1}$ = 0.09071 mm/year).

To simulate a scenario at the operating temperature (T_2 = 145 °C), the adapted Arrhenius equation is used:

$$V_{Cg,2} = V_{Cg,1} \cdot exp\left[\frac{E_a}{R} \cdot \left(\frac{1}{T_1} - \frac{1}{T_2}\right)\right] \quad (4)$$

where: V_{Cg} represents the corrosion rate; E_a is the apparent activation energy of the corrosion process (J/mol); R is the universal ideal gas constant (8.314 (J/(mol·K)); T is the temperature (in K).

For carbon steels in alkaline/neutral aqueous solutions, the apparent activation energy E_a is controlled either by the chemical activation reaction (E_a = 30 … 40 kJ/mol) or by the diffusion of dissolved oxygen through the film (E_a = 15 … 20 kJ/mol), [15–17].

The diffusion-controlled case (assuming E_a = 20 kJ/mol): according to equation (4), by substituting the known values, the corrosion rate$V_{Cg,2}$ at the temperature (T_2 = 145 °C) is obtained as $V_{Cg,2} \approx 1.0\ mm/year$.

From a structural perspective, this accelerated dynamic implies a major risk of premature and severe reduction in the shell wall thickness, significantly diminishing the remaining useful life of the equipment within only a few years of continuous operation.

Corrosion behavior of X2CrNiMo17-12-2 steel in fluid F1 (1632-hour test)

Experimental analysis of the specimens made of X2CrNiMo17-12-2 austenitic stainless steel, subjected to a long-term immersion test (1632 hours) at ambient temperature in the F1 working medium, demonstrates high corrosion resistance. The average corrosion rate, determined gravimetrically after the removal of corrosion products according to the ISO 8407 standard, is V_{Cg} = 0.00853 mm/year (Table 5). According to standardised chemical resistance scales (correlated with NACE SP0775-2023 and ISO 9226-2012 classifications), a corrosion rate below the critical threshold of 0.01mm/year classifies the material within the excellent resistance category (completely stable material / negligible corrosion), [14].

a. *Macroscopic analysis of the surfaces of the studied specimens*.

- *Upon macroscopic examination***,** the surface of the X2CrNiMo17-12-2 steel specimens retains its initial shiny metallic appearance, with no colour changes detectable by the naked eye. No deposits of rust, friable oxides, or crusts are observed on any area of the specimen (Figure 7).
- *The surface is homogeneous***.** No traces of pitting (corrosion pits) or exfoliation are detected, a phenomenon due to the stability of the passive chromium oxide (Cr_2O_3) film, which was effectively protected against the 34.08 mg/l of chlorides by the molybdenum content within the material. Macroscopically, the material is classified among those unaffected by the medium.

b. *Correlation between the medium composition (F1) and the mechanical effects on X2CrNiMo17-12-2 steel*. X2CrNiMo17-12-2 steel

demonstrates superior structural stability in the F1 medium, ensured by the combination of chromium, molybdenum, and nickel, which generates high passivation against chlorides and inhibits hydrogen diffusion. This behaviour guarantees the maintenance of mechanical integrity, including ductility and the load-bearing cross-section, providing resistance to both corrosion and cracking.

c. Extrapolation of laboratory results to real operating conditions – maximum allowable pressure of 2.4 MPa, maximum allowable temperature of 145 °C.

To extrapolate the laboratory results to real operating conditions, the adapted Arrhenius equation (equation 4) is utilized.

The corrosion rate determined in the laboratory at ambient temperature ($T_1 \approx 20^0$C $\approx$ 293.15 K) is low ($V_{Cg,1}$ = 0.00853 mm/year).

In the absence of an experimentally determined activation energy (E_a), the literature [15] indicates an average value of $E_a \approx$ 40000 J/mol for the active dissolution of austenitic steels in weakly acidic/neutral media.

According to equation (4), by substituting the known values, the corrosion rate $V_{Cg,2}$ at the temperature T_2 = 145 ^{0}C de $V_{Cg,2} \approx 0.86\ mm/year$.

Regarding the operating pressure of 2.4 MPa (24 bar), it maintains the F1 medium in a liquid state at 145 °C (preventing boiling, as the water saturation pressure at 145 °C is approximately 0.41 MPa). However, this combination radically alters the chemical equilibria.

Utilizing direct extrapolation ignores the fact that the corrosion mechanism changes radically from cold to hot conditions.

At the parameters (145 °C and 2.4 MPa), the corrosion triggers for X2CrNiMo17-12-2 steel are the chloride concentration, tensile mechanical stresses, and the presence of dissolved oxygen, which together activate the stress corrosion cracking mechanism. Directly extrapolating the low-temperature behavior (where the steel is passive and stable) to these high-temperature and high-pressure conditions radically changes the degradation mechanism from a controllable localized corrosion into sudden and catastrophic cracking.

The laboratory results ($V_{Cg,1} \approx$ 0.00853 mm/year) cannot be used to guarantee the equipment's service life at 145 °C and 2.4 MPa. The extrapolation indicates a transition from a safe regime to one with a high risk of stress corrosion cracking (SCC) and under-deposit pitting, as detailed in section 5 on actual industrial samples.

5. Degradation assessment on real industrial samples

The following section presents the experimental research conducted on specimens sampled directly from the shell and tubes, following repair and overhaul works performed on the analysed equipment.

Case 1. **Equipment: tubes, material: P265GH, working medium: F1, operating conditions: maximum allowable pressure: 2.4 MPa, maximum allowable temperature: 145°C**

The tubes represent the most exposed component of a heat exchanger, featuring reduced wall thicknesses (5…7 mm) to facilitate heat transfer, which makes them extremely sensitive to degradation. Tube coupons were extracted from various critical zones of the heat exchanger (Figure 8).

Fig. 8. Tube sampling.

A. Visual and macroscopic appearance

Macroscopic examination of the samples taken from the heat exchanger tube bundle, sample 1, indicates severe localised pitting corrosion on the outer surface of the tubes (Figure 9).

For sample 2, macroscopic and morphological analysis reveals the presence of massive exogenous deposits in the form of adherent crusts (Figure 10). These exhibit a compact, dense, and apparently homogeneous macro-structural appearance on the surface; however, from a mechanical standpoint, they manifest low internal cohesion at the interface with the base metal, being easily detached through light mechanical stress (manual peeling or gentle scraping).

Unlike sample 1, no localised degradation phenomena are observed beneath these deposits; there are no corrosion cavities, deep crevices, or

microscopic pits (pitting) on the adjacent metal surface. This morphology indicates that the compact crust layer acted locally as a shielding physical barrier, limiting the diffusion of aggressive chemical elements from the F1 medium towards the ferritic-pearlitic matrix, thereby preventing the initiation of the localised electrochemical attack beneath the sediment.

Fig. 9. Aspects of pitting corrosion and under-deposit corrosion (crevice and pitting cavities) – sample 1.

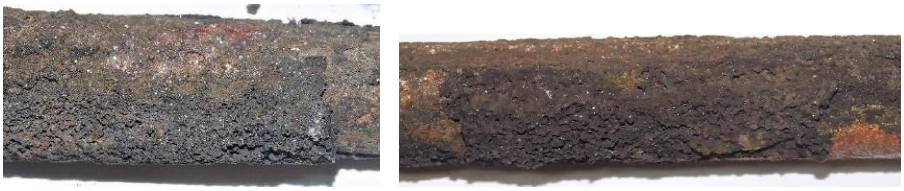

Fig. 10. Corrosion aspects – sample 2

B. Macroscopic and microscopic appearance in cross and longitudinal sections

Structural analysis of the P265GH steel tubes reveals a fine and homogeneous ferritic-pearlitic microstructure (Figures 11 and 12), with the actual ferritic grain size corresponding to grain size number 9 (according to

SR EN ISO 643), which is characteristic of a correctly executed normalising heat treatment. The metal matrix is dominated by polyhedral grains of equiaxed ferrite with well-defined and clean boundaries. The pearlitic zones are distributivity isolated, primarily as fine lamellar colonies located at the corners and boundaries of the ferrite grains, at triple junctions. The non-metallic inclusions (such as silicates or manganese sulphides) are low in number and finely dispersed within the matrix, falling within the purity limits specific to quality steels for pressure equipment.

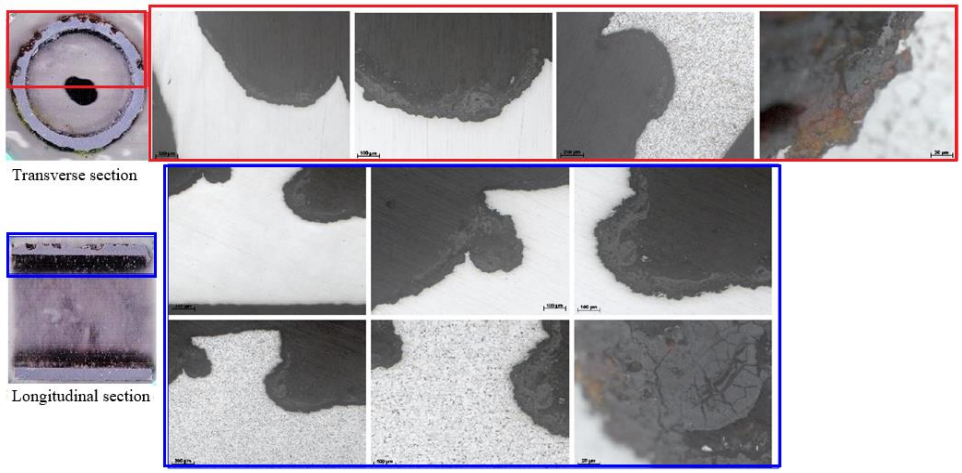

Fig. 11. Microscopic aspects – sample 1.

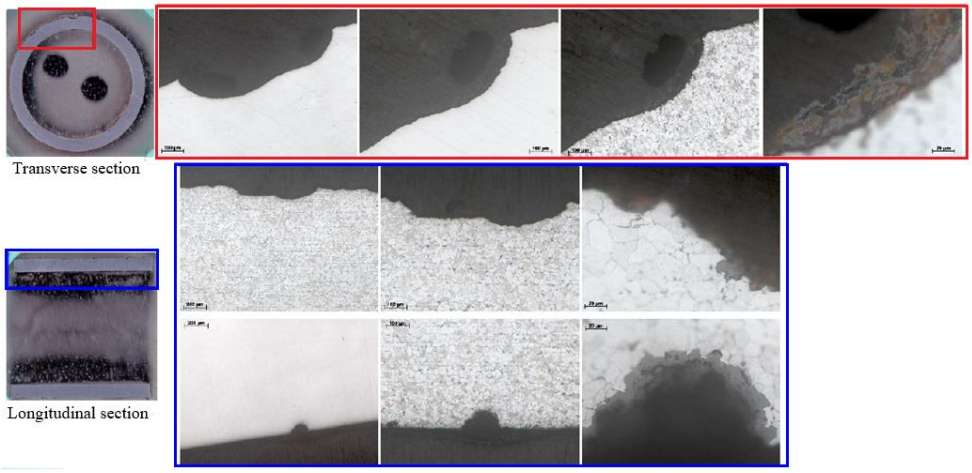

Fig. 12. Microscopic aspects – sample 2.

From the standpoint of degradation, severe manifestations of under-deposit corrosion (crevices and pitting cavities) and pitting are observed. Under the nominal operating conditions of the exchanger (maximum pressure of 2.4 MPa and temperature of 145 °C), this unalloyed ferritic-pearlitic microstructure exhibits critical vulnerability, as the F1 corrosive medium circulates along the exterior of the tubes. The elevated temperature of 145 °C exponentially accelerates the transgranular electrochemical attack within the majority ferritic phase, transforming the small initial pits into deep and irregular cavities.

Simultaneously, the external pressure of 2.4 MPa exerts compressive mechanical stresses. As the under-deposit corrosion and pitting cavities reduce the wall thickness, massive geometric stress concentrators are created. This mechano-chemical synergy leads to the rapid advancement of the degradation, ultimately resulting in the complete breakthroughs identified on the samples.

C. SEM/EDS analyses on the collected deposits

Advanced investigation using scanning electron microscopy (SEM) coupled with energy-dispersive X-ray spectroscopy (EDS) of the solid deposits collected from the studied samples enabled the determination of the elemental chemical composition and the crystalline phases present (Figure 13).

Point and area compositional microanalyses reveal a complex structure of the crusts, characterized by the coexistence of the native corrosion products of the carbon steel with exogenous substances crystallized from the F1 working medium:

- Iron and silicon oxides. The massive presence of iron oxides confirms the continuous oxidation of the ferritic-pearlitic matrix. These are interspersed with silicon oxides (silica), likely introduced as suspended solid particles or impurities from the process fluid, which contribute to the compact appearance of the crust.
- Sodium, calcium, and iron chlorides. The identification of chlorides (NaCl, $CaCl_2$, and $FeCl_2/FeCl_3$) within the bulk of the deposit provides direct chemical evidence of the aggressiveness of the F1 medium. Chloride ions (Cl^-) possess high penetration and diffusion capacities; they locally breach the oxide layers and induce the severe pitting observed in sample 2. The presence of iron chloride indicates an advanced stage of anodic attack on the iron within the P265GH steel, while sodium and calcium chlorides originate directly from

the evaporative concentration of salts from the fluid onto the hot surface of the tube (145 °C).

a – sampling area

b – deposit outer appearance (medium interface)

c – deposit inner appearance (material interface)

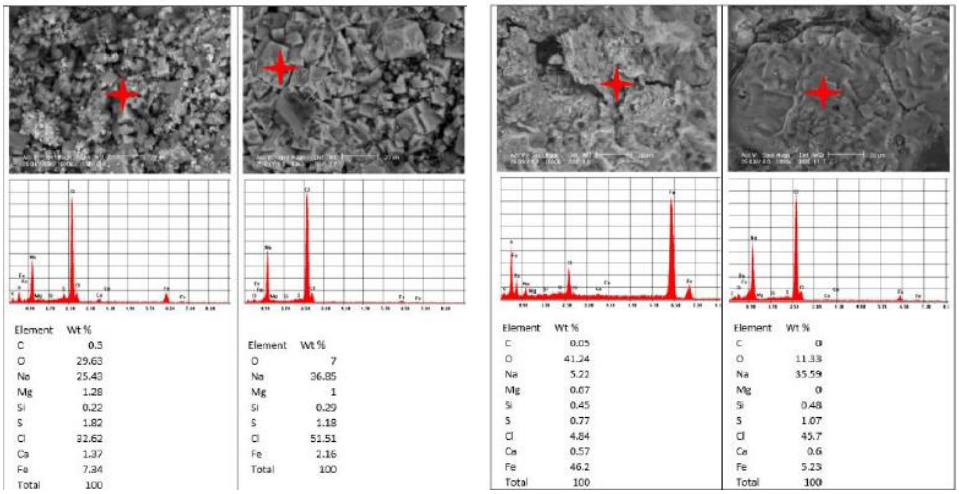

d – exterior (medium interface) *e – interior (material interface)*

Fig. 13. SEM/EDS analyses on the collected deposits – sample 2.

- Sulphur and iron sulphides. The detection of sulphur and iron sulphides indicates additional degradation through the interaction of the steel with active sulphur-based compounds from the F1 medium. The formed iron sulphides are typically cation-deficient, highly electrically conductive, and exhibit lattice defects, transforming into local cathodic sites that accelerate the dissolution of the adjacent ferrite, thereby enhancing under-deposit corrosion and macroscopic cavity phenomena.

In conclusion, the SEM/EDS data demonstrate that the accumulated deposits do not merely constitute an inert residue, but rather a complex reactive medium. Within this medium, the accumulation of chlorides and sulphides maintains a highly corrosive and locally acidic under-deposit

microenvironment, explaining the severe structural degradation of the tube bundle.

Technical recommendation

Based on the macroscopic and microstructural analyses, as well as the evaluation of the operating regime (2.4 MPa, 145 °C, external F1 medium), the following technical and organizational measures are formulated:

1. *Material replacement* (primary recommendation). It is recommended to discontinue the use of P265GH unalloyed carbon steel for the tube bundle and replace it with X2CrNiMo17-12-2 high-alloy austenitic stainless steel. Its stable austenitic structure and molybdenum content (2.0…2.5%) will ensure high passivation, pitting resistance in the presence of chlorides, and total resistance to the reduction of the load-bearing cross-section.

2. *Short-term non-destructive monitoring* (if P265GH is retained). If the replacement of the tube bundle is not immediately feasible, it is mandatory to implement a periodic inspection programme using Eddy Current Testing (ECT) at intervals of maximum (6…12) months. This method will detect and monitor wall thinning and external cavities from the inside before they reach the critical thickness for structural collapse.

Case 2. **Equipment: shell, material: P265GH, working medium: F1, operating conditions: maximum allowable pressure: 2.4 MPa, maximum allowable temperature: 145°C**

The correlation of laboratory data with the nominal operating parameters of the real plant shell (p_{max} = 2.4 MPa, t_{max} = 145 °C) highlights a state of high structural vulnerability for the P265GH steel. Although from a mechanical point of view the material corresponds to the pressure class, the temperature of 145 °C will exponentially accelerate the corrosion kinetics determined experimentally at ambient temperature ($V_{Cg,P}$ = 0.09071 mm/year). Moreover, the association between the mechanical stresses generated by the pressure of 2.4 MPa and the presence of active agents (chlorides, sulphides, ammonium) places the P265GH steel in an area with a high risk of failure by stress corrosion cracking (SCC) and hydrogen embrittlement. These phenomena determine an accelerated thinning of the shell wall, prematurely reducing the load-bearing section below the safety limits imposed by the thermobaric regime of the plant.

A. Visual and macroscopic appearance

Direct visual examination and macroscopic analysis of the surfaces of the heat exchanger shell (manufactured from P265GH grade carbon steel) revealed an advanced and severe stage of surface structural degradation. The chemical-mechanical wear phenomena are unevenly distributed, primarily affecting extensive areas located in the lower section of the shell. Through gravitational sedimentation, this lower region promotes fluid stagnation and the massive accumulation of the previously identified reactive deposits and crusts (chlorides, sulphides, and silicates), thereby maintaining a highly aggressive local microenvironment in contact with the metal wall.

The primary morphology of the degradation manifests as an irregular surface topography, characterised by (Figure 14):

• *Localized corrosion pitting*. High density of active micro-cavities, with hemispherical geometry, oriented perpendicular to the metal wall. These represent electrochemical initiation points where the passive oxide layer has been locally penetrated by active chlorine and sulphur ions from the dissociation of salts present in the F1 medium.

• *Macroscopic corrosion craters and caverns*. By the union of adjacent pits and under the action of fluid hydrodynamics, extensive corrosion cavities have developed under the layer. Profilometric and ultrasonic measurements performed in these indicated areas record critical penetration depths, ranging between 2.0 mm and 3.0 mm.

a *b* *c*

Fig. 14. Shell – visual appearance:
a – decommissioned shell; *b, c* – sample cut from the shell.

Given the initial nominal thickness of the shell wall of 12.0 mm, these geometric defects represent a massive local loss of the load-bearing section, up to 25% of the total design thickness.

Under the nominal and maximum operating conditions of the equipment (maximum allowable pressure of 2.4 MPa and maximum temperature of 145 °C), this sharp reduction in the wall represents a critical risk of structural failure through loss of pressure stability.At a temperature of 145 °C, the yield strength of P265GH steel is reduced, and the presence of 3 mm craters generates major mechanical stress concentrators (membrane and local bending stresses), jeopardizing the safe operation of the entire heat exchanger.

B. Macroscopic and microscopic appearance

Optical metallographic analysis performed on samples taken from the shell wall (P265GH grade carbon steel) reveals a ferrite-pearlite microstructure typical of a normalized state (Figure 15). The metallic matrix exhibits a high degree of structural homogeneity, consisting predominantly of a ferritic phase formed by well-defined equiaxed polyhedral grains. The secondary pearlitic constituent is present in a low volume fraction and is unevenly distributed in the form of strings or bands.

From a degradation standpoint, this banded orientation of the pearlite at the microscopic level constitutes a structural vulnerability in the presence of the F1 environment and a temperature of 145 °C. The interface between the pearlite strings and the adjacent ferritic matrix creates local galvanic micro-cells, promoting preferential corrosion propagation along these alignments. This mechanism explains the morphology of the extensive craters identified macroscopically in the lower section of the shell.

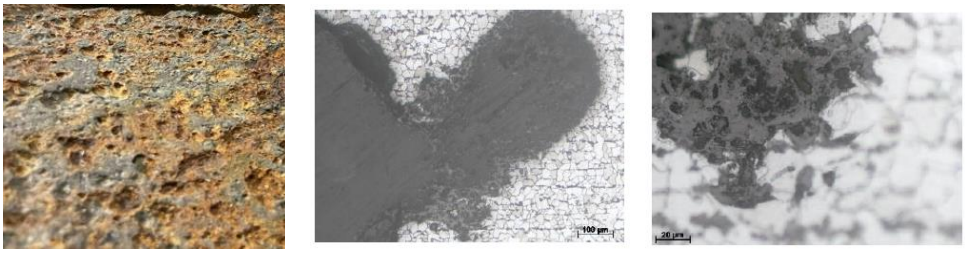

a b

Fig. 15. Shell – macroscopic and microscopic appearance:
a – macroscopic appearance; *b* – microscopic appearance.

C. SEM/EDS Analysis

Scanning electron microscopy (SEM) coupled with energy-dispersive X-ray spectroscopy (EDS) investigation reveals (Figure 16) the presence of sodium, iron, and calcium chlorides, iron and silicon oxides, as well as sulphur (iron sulphides).

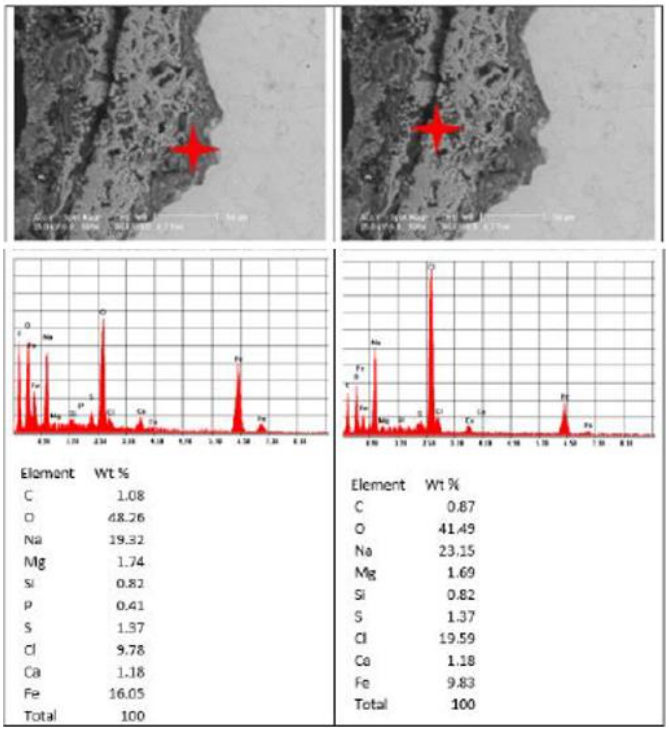

Fig. 16. Shell – SEM/EDS analysis.

EDS spectra obtained through area scans and point analysis reveal a heterogeneous and reactive structure, characterized by the coexistence of endogenous corrosion products (derived from the degradation of the metallic matrix) with exogenous substances, which crystallized and concentrated from the F1 process fluid at the operating temperature of 145 °C. Thus, the SEM/EDS analysis demonstrates that the complex mixture of water-soluble chlorides, stable oxides, and semiconducting sulphides transforms the settled crusts into an actively chemical reservoir. This reservoir isolates the metallic surface from the action of any potential system inhibitors, maintains a high local acidity, and explains the formation of the (2…3) mm deep craters detected in the lower section of the shell and on the outer walls of the tubes.

6. Conclusions

By corroborating the long-term laboratory test results with the complex analyses performed on actual industrial components, the following conclusions regarding the technical condition and structural optimization solutions for the heat exchanger were formulated:

a) Determination of the corrosion rate through long-term laboratory tests:

- *Insufficient corrosion resistance of P265GH carbon steel*. Long-term corrosion tests confirm a high corrosion rate of P265GH steel in contact with the F1 working fluid. The absence of passivating alloying elements directly exposes the ferrite-pearlite matrix to continuous electrochemical attack, enhanced by the operating temperature of 145 °C. The lack of a stable protective film indicates that this material does not possess the necessary chemical resistance to ensure the designed equipment lifespan in the presence of the F1 fluid.
- *Superior performance of X2CrNiMo17-12-2 (AISI 316L) steel*. Laboratory investigations demonstrate the high resistance of this steel grade, its corrosion rate being negligible (practically within the chemical immunity range). The massive presence of chromium and nickel, combined with the contribution of (2.0…2.5) % molybdenum, ensures the formation of a highly dense, self-healing passivation layer. This layer effectively blocks the penetration of aggressive chlorine and sulphur anions, confirming X2CrNiMo17-12-2 steel as an optimal and reliable technical solution for the complete replacement of the exposed structural elements.

b) Evaluation of degradation on actual industrial samples:

- *Cumulative degradation kinetics through the correlation of mechano-corrosive stresses.* The analysis of specimens taken directly from the tubes and the heat exchanger shell highlights severe localized degradation phenomena such as pitting, crevice corrosion, and macroscopic caverns. In the lower section of the shell, deep craters of (2.0…3.0) mm were recorded (representing a loss of up to 25% of the load-bearing cross-section). Wall thinning under a pressure of 2.4 MPa and a temperature of 145 °C generated massive stress concentrators, triggering material perforations.
- *Autocatalytic nature of solid deposits.* Advanced SEM/EDS microanalysis of the collected crusts proves that the deposits are not inert but function as an acidic saline screen. The accumulation of sodium, calcium, and magnesium chlorides, alongside iron sulphides, maintains high local moisture

and acidity beneath the layer. This micro-environment isolates the metal from any potential system inhibitors and exponentially accelerates the anodic dissolution kinetics of the P265GH steel, explaining the behavioral differences between sample 1 (caverns beneath the porous layer) and sample 2 (temporarily screened by a compact crust, but subject to the same long-term risk).

- *Macroscopic validation of passivation kinetics.* Macroscopic analysis validates the hypothesis of the passivation kinetics of X2CrNiMo17-12-2 steel, whose surface remains inert in the F1 environment, unlike P265GH steel, where the lack of protective alloying elements leads to severe macroscopic degradation through general corrosion and porous oxide accumulation.
- *Metallurgical validation of the structural upgrade.* The experimental results metallurgically validate the opportunity of using X2CrNiMo17-12-2 stainless steel as an upgrade solution for the heat exchanger shell instead of carbon steel (P265GH). At ambient temperature and within the specified chemical environment, the material maintains its passivated state, ensuring a minimal degradation rate and a high service life forecast.

REFERENCES

[1] *R. K. Shah, and D. P. Sekulic,* "Fundamentals of heat exchanger design", John Wiley & Sons, ISBN: 0-471-32171-0, 2003

[2] *A. Petrov,* "Types of heat exchangers in industry, their advantages and disadvantages, and the study of their parameters", IOP Conference Series Materials Science and Engineering 963 (1):012027, November 2020, DOI: 10.1088/1757-899X/963/1/012027

[3] *Y. Hua, W. Taleb, T. Chapentier, R. Barker, et al*., "Localized and General Corrosion Characteristics of Carbon Steel in H_2S Environments", Paper presented at the CORROSION 2019, Nashville, Tennessee, USA, March 2019, https://onepetro.org/NACECORR/proceedings-abstract/CORR19/CORR19/NACE-2019-12943/127190

[4] *M. Sagara, M. Ueyama, H. Amaya, Y. Suzuki*, "Evaluation of the Surface on CRA After the Actual Exposure in Sour Gas Well", Paper presented at the CORROSION 2019, Nashville, Tennessee, USA, March 2019, https://onepetro.org/NACECORR/proceedings-abstract/CORR19/CORR19/NACE-2019-12946/127220

[5] *K. Mizushima, N. Satake, M. Sakai, J. Miyashita*, "Factors for Selecting Thermal Insulation Materials to Prevent Corrosion Under Insulation", *Paper presented at the CORROSION* 2019, Nashville, Tennessee, USA, March 2019, https://onepetro.org/NACECORR/proceedings-abstract/CORR19/CORR19/NACE-2019-12952/127202

[6] *S. Soltaninia, Z. Ardaniel, C. Shargay, S. Radovcich*, "Heat Treatment of Heat Exchanger U-Bends – Practices on Different Materials and Case Histories of Failures", Paper presented at the AMPP Annual Conference and Expo, New Orleans, Louisiana, March 2024, https://onepetro.org/amppcorr/proceedings-abstract/AMPP24/AMPP24/AMPP-2024-20815/556825

[7] *C. Chauvet, C. Meynet, F. Maktar*, "How CFD Can Help to Understand Corrosion in Heat Exchanger", Paper presented at the Abu Dhabi International Petroleum Exhibition & Conference, Abu Dhabi, UAE, November 2019, Paper Number: SPE-197722-MS, https://doi.org/10.2118/197722-MS

[8] *J. Xie, K. Yazdanfar, M. Butcher, T. Rockwell*, "Corosiune of a Shell-and-Tube Heat Exchanger", Paper presented at the CORROSION 2013, Orlando, Florida, March 2013, Paper Number: NACE-2013-2118, https://onepetro.org/NACECORR/proceedings-abstract/CORR13/CORR13/NACE-2013-2118/121325

[9] *Z. Mahidashti, M. Rezaei, S. Eftekhari*, "A corrosion failure analysis of heat exchanger tubes operating in petrochemical refinery", Engineering Failure Analysis 119, October 2020, DOI: 10.1016/j.engfailanal.2020.105011

[10] *G. Siegmund, G. Schmitt, J. Noga*, "Cracking Resistance of Alloy 904 L in Brine under Highly Sour Conditions" Proceedings of the CORROSION 2014. CORROSION 2014, San Antonio, TX. (pp. 1-10), March 9–13, 2014, AMPP. https://doi.org/10.5006/C2014-4061

[11] *G. Siegmund, G. Schmitt, J. Noga*, "SSC Resistance of 316Ti in Brine under Highly Sour Conditions" Proceedings of the CORROSION 2013. CORROSION 2013, Orlando, FL. (pp. 1-10), March 17–21, 2013, AMPP. https://doi.org/10.5006/C2013-02698

[12] *V. P. Tudorache, M. Stan, L. Avram, N. N. Antonescu*, "Elements for the preventing and combating corrosion to cylindrical metal tank for destined storage of liquid hydrocarbons", EMERG - Energy Environment Efficiency Resources Globalization, Vol. 7, Issue 3, January 2021, https://doi.org/10.37410/ EMERG.2021.3.08

[13] *S. Adair, P. A. Attwood*, "In-service stress corrosion cracking of AISI 316L stainless steel in an H_2S environment"**,** Corrosion Engineering Science and Technology 49(5):396-400, August 2014, DOI: 10.1179/1743278213Y.0000000141

[14] *A. Jaragh, A. W. Al-Ahmad et al*., "Internal Corrosion Severity Ranking of Crude Oil Pipelines", Conference: SPE Kuwait Oil & Gas Show and Conference, October 2019, DOI: 10.2118/198133-MS

[15] *M. G. Fontana*, "Corrosion Engineering" (3rd ed.). McGraw-Hill, 1986.

[16] *D. A. Jones*, "Principles and Prevention of Corrosion" (2nd ed.), Prentice Hall, 1996

[17] *P. R. Roberge*, "Corrosion Engineering: Principles and Practice", McGraw-Hill Professional, 2008

Authors' biographies

Mihai OPREA is a PhD student at the Petroleum-Gas University of Ploiesti, where he also earned his BSc (2017) and MSc (2019) in petroleum equipment engineering. Professionally, he serves as an Inspection and Integrity Expert within the technical authority team at OMV Petrom. He brings 9 years of experience in integrity management for mechanical equipment, pipelines, and pressure vessels across the oil & gas, petrochemical, hydrogen, and water treatment sectors. His role focuses on overseeing mechanical design for major capital projects (EPC/EPCM) and approving technical documentation for refinery modernization.

E-mail: oprea_mihai94@yahoo.com

Ion NAE holds a PhD in Mechanical Engineering and is a Full Professor and Ph.D. coordinator at Faculty of Mechanical and Electrical Engineering of the University Petroleum-Gas of Ploiesti, Romania. Fields of scientific research: applied research on the construction, manufacture, operation and durability of petroleum equipment, manufacturing systems, production systems management, project management, research-development-innovation management. Member of professional associations: Romanian Association of Fracture Mechanics (ARMR), Romanian Association of Tribology (ART), General Association of Romanian Engineers (AGIR).

E-mail: inae@upg-ploiesti.ro

Gabriela Cristina IONESCU holds a Ph.D. in Mechanical Engineering and is an Associate Professor at the Petroleum-Gas University of Ploiesti, Romania. Her teaching and research activities focus on oil, gas, and petrochemical equipment. She analyzes manufacturing, construction, and maintenance processes to enhance the durability and tribological behavior of industrial machinery. Furthermore, she has contributed to numerous scientific publications in prestigious journals and participated in research projects focused on sustainable materials, process optimization, and advanced manufacturing technologies.

E-mail: ionescug@upg-ploiesti.ro

Răzvan George RÎPEANU holds a Ph.D. in Mechanical Engineering and is Full Professor and Ph.D. adviser at The Mechanical and Electrical Faculty of Petroleum-Gas University of Ploiesti, Director of the University Doctoral Studies Council. He was President of of the Romanian Tribological Association and in the present was elected Vice-President. His research is focused mainly on increasing durability of petroleum and gas equipment by analyzing manufacturing technology, construction, and maintenance to improve their tribological behavior. It is full member of Technical Sciences Academy of Romania and was awarded by CNR of CME with medal in 2024.

E-mail: rrapeanu@upg-ploiesti.ro

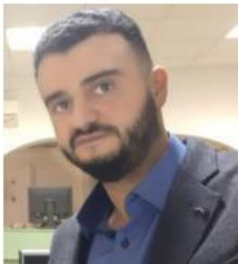

Ibrahim Naim RAMADAN holds a Ph.D. in Mechanical Engineering, is Associate Professor at Petroleum-Gas University of Ploiesti, Romania. His research topics include Material Science, Machine Parts, Corrosion of Transport and Storage Equipment, Materials for Hydrocarbons Distribution Systems, Refinery equipment construction and Maintenance Technology, Oil Equipment Reconditioning Techniques, Steel and HDPE pipes Destructive Testing and also Materials Testing and Characterization for Additive Manufacturing.

E-mail: ibra@upg-ploiesti.ro